Energy dependence of pion inelastic scattering from ^{208}Pb

D. S. Oakley*
University of Colorado, Boulder, Colorado 80309
and Lewis and Clark College, Portland, Oregon 97219

R. J. Peterson
University of Colorado, Boulder, Colorado 80309

S. J. Seestrom, C. L. Morris, and M. A. Plum
Los Alamos National Laboratory, Los Alamos, New Mexico 87545

J. D. Zumbro†
University of Pennsylvania, Philadelphia, Pennsylvania 19104

A. L. Williams, M. A. Bryan, J. W. McDonald, and C. Fred Moore
University of Texas at Austin, Austin, Texas 78712
(Received 20 June 1991)

Differential cross sections were measured for pion elastic and inelastic scattering from ^{208}Pb at $T_\pi = 120$ and 250 MeV. Energy-dependent neutron- and proton-transition matrix elements for a range of excited states were extracted and tested for consistency, using several structure models.

I. INTRODUCTION

A comparison of π^+ and π^- inelastic scattering allows an isospin separation of nuclear transitions into contributions from neutron- and proton-transition matrix elements, M_n and M_p. Absolute values of these quantities have been shown to agree with electromagnetic determinations of M_p and with other determinations of both M_n and M_p for very collective transitions such as to the lowest-lying 2^+ and 3^- states of light- and medium-mass doubly even nuclei [1–6]. In some of these examples the extracted ratios of M_n/M_p have been found to be constant with respect to changing incident pion energy over the interval $T_\pi = 100$–300 MeV. An analysis of data for pion inelastic scattering to the giant resonance region of the heavier ^{208}Pb nucleus, however, yielded an unexpectedly large ratio[7] of M_n/M_p. Unlike the case for low-lying levels in lighter nuclei, the ^{208}Pb giant resonance value for M_n/M_p is not in agreement with that from neutron and proton scattering; for those probes the extracted value of M_n/M_p is closer to the N/Z expectation of the collective model [8,9].

In the present work pion inelastic scattering to a number of low-lying transitions in ^{208}Pb has been measured at two incident pion energies in order to test the general validity of the model used to extract isospin matrix elements in heavy nuclei. For the strong 3_1^- state an analysis of earlier data at other energies is also presented. The extracted matrix elements should be independent of the initial beam energy, and any energy dependence of these matrix elements would indicate an inadequacy of either the presumed transition density model or the reaction mechanism.

Doubly magic ^{208}Pb exhibits a number of transitions that are experimentally resolvable (at our resolution near 150 keV) and these have been extensively studied, both theoretically and experimentally [7–18]. Previous pion-scattering experiments [12–14] have measured elastic scattering on this nucleus and there are some limited data for the first 3_1^- state, but no energy-dependent (T_π) pion data exist to demonstrate consistency. The present experiment is therefore carried out at two beam energies (120 and 250 MeV), symmetrically below and above the centroid of the $\Delta_{3/2,3/2}$ resonance, to test the reaction and structure models.

II. EXPERIMENTAL DETAILS

Data were collected using the Energetic Pion Channel and Spectrometer (EPICS) system at the Los Alamos Clinton P. Anderson Meson Physics Facility (LAMPF). The momentum-dispersing channel was tuned to select the incoming pion sign and energy and a high-resolution spectrometer measured the outgoing particle momentum, as for many of the previous high-resolution pion-scattering experiments. A pion energy-loss spectrum obtained at $T_\pi = 120$ MeV is shown in Fig. 1. Data were obtained at scattering angles between $\theta_{lab} = 12°$ and 48° at incident pion energies of 120 and 250 MeV. The ^{208}Pb target had an areal density of 107.1 mg/cm^2 and was greater than 99.7% isotopically and chemically pure, yielding an experimental energy resolution of 150 keV (FWHM). The data were normalized by comparing yields for π^+ scattering from hydrogen to cross sections calculated from known π-p phase shifts [19]. The uncertainty in this normalization was ±8%.

 ©1991 The American Physical Society

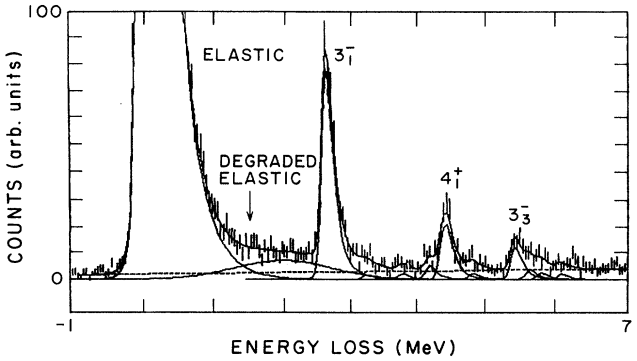

FIG. 1. Negative pion energy-loss spectrum (fitted) at $\theta_{lab}=33°$ and $T_\pi=120$ MeV.

Peak areas were extracted from the pion energy-loss spectra with the relative energy separations of the various states constrained by the known excitation energies [20]. Peaks from states within 60 keV of one another were fitted as a single peak. Resolved peaks were fitted at 2.61, 4.70, and 5.30 MeV (3^- states); 3.20, 3.71, and 3.96 MeV (5^- states); 4.09, Mev (the 2_1^+ state); 4.32 MeV (the 4_1^+ state); and at 4.42 MeV (the 6_1^+ state). The 3.96 MeV 5_3^- peak was not seen strongly enough to allow an analysis. Electron scattering to this state shows a weak and largely transverse excitation [10]. Strong peaks were also observed at 5.50, 5.70, and 6.00 MeV, but the density of states is high at this excitation and the featureless angular distributions indicate that no single state dominates these peaks. A secondary elastic peak, as described in Ref. [2], can also clearly be seen in Fig. 1. A typical fit is plotted with the data in Fig. 1.

III. ELASTIC ANALYSIS AND RESULTS

Our elastic-scattering data were compared to calculations from the computer code DWPI [21], using the distorted-wave impulse approximation (DWIA). All calculations used the Kisslinger [22] form for the pion-nucleus potential with an empirical energy shift [23] of -28.0 MeV and no second-order effects. The neutron and proton ground-state densities, ρ_n and ρ_p, were parametrized with a Woods-Saxon distribution where the proton half-density radius and the root-mean-square (rms) charge radius $\langle r^2\rangle_z^{1/2}$ were from previous pion data [7]. These parameters were modified from the charge-density parameters determined by electron scattering to remove the finite size of the proton charge distribution. The neutron parameters were initially taken to be the same as the proton parameters but were also varied to obtain the best fit to the elastic-scattering data.

The elastic angular distributions measured here are shown in Figs. 2 and 3. These data are reproduced well by calculations using half-density radii, $c_p=c_n=6.51$ fm, and diffuseness, $z_p=z_n=0.55$ fm (which give rms neutron and proton radii of 5.44 fm). The agreement with the π^- data is slightly improved by increasing the diffuseness of the neutron distribution from 0.55 to 0.65 fm. This cor-

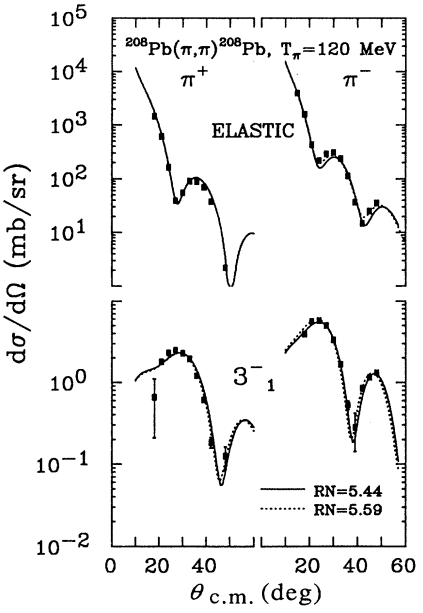

FIG. 2. Elastic-scattering and 3_1^- inelastic-scattering angular distributions from ^{208}Pb $(\pi,\pi)^{208}$Pb at $T_\pi=120$ MeV. The solid curves represent DWPI calculations (with the Tassie model for the 3^- state) with $c_n=c_p=6.51$ fm and the dotted curves show calculations with z_n increased from 0.55 to 0.65 fm.

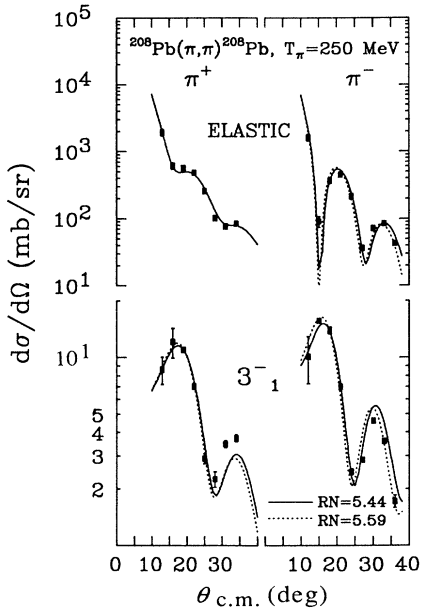

FIG. 3. Elastic-scattering and 3_1^- inelastic-scattering angular distributions from ^{208}Pb $(\pi,\pi)^{208}$Pb at $T_\pi=250$ MeV. The solid curves represent DWPI calculations (with the Tassie model for the 3^- state) with $c_n=c_p=6.51$ fm and the dotted curves show calculations with z_n increased from 0.55 to 0.65 fm.

responds to an increase of the rms neutron radius to 5.59 fm. Any further increase in the neutron radius, however, would fail to reproduce the observed shapes at the two beam energies. Because this change has no major effect on the outcome of the inelastic calculations and for consistency with other ^{208}Pb$(\pi,\pi')^{208}$Pb experiments [12–14], the neutron parameters were left the same as those for the proton for the analysis to follow.

IV. INELASTIC ANALYSIS AND RESULTS

The code DWPI was also used to calculate the inelastic-scattering cross sections. The data for all transitions were compared to calculations using surface peaked collective-model transition densities, using the vibrational model derivative of the ground state, $\rho_{\rm tr}\sim\beta d\rho/dr$, as well as the Tassie model, $\rho_{\rm tr}\sim\beta r^{l-1}d\rho/dr$ [2,24]. The strengths of the transitions in both models are characterized by the deformation parameters β. The Tassie model generally represents the correct transition density shape for strong, sum rule-satisfying giant-resonance excitations [24,25], while strong low-lying states, particularly the 3_1^- state in ^{208}Pb, may better be described as vibrations [26]. Fourier-Bessel analyses of electron-scattering data [10] confirm that the states treated in the present work do indeed have proton transition densities peaked at the nuclear surface, confirming the features of these collective models.

This choice of collective transition densities also allows a measurement of matrix elements which is consistent with other pion-scattering analyses [7,12–16]. In the collective model we expect $M_n/M_p=N/Z$, with neutron and proton matrix elements, M_n and M_p, related to the neutron and proton strength (deformation) parameters, β_n and β_p, by

$$M_p\equiv Z\int r^{l+2}\rho_{{\rm tr},p}(r)dr/4\pi\ ,$$

for instance. In the analysis presented here, the deformation parameters were varied until simultaneous agreement was obtained with the π^- and π^+ data.

For the first 2^+ state we also compare our data to theoretical predictions using transition densities from random-phase-approximation (RPA) calculations, taken from Ref. [27], where the shape of the neutron-transition density is very different from that for the proton. M_n/M_p is about the same as the ratio of the π^- to π^+ cross sections, ignoring distortions, if the shapes of the neutron- and proton-transition densities are the same. Differences between the neutron- and proton-transition densities in the surface can result in the cross-section ratio being different from the ratio of matrix elements because the π-nucleus interaction occurs mostly in the nuclear surface.

Coulomb excitation should not be neglected for a high-Z nucleus and is included in the calculations presented here. The details of the resulting Coulomb-nuclear interference and its effect on pion scattering have been given in Ref. [16].

V. INELASTIC SCATTERING DATA AND ANALYSIS

Data for the 3_1^- state obtained at $T_\pi=120$ and 250 MeV are plotted in Figs. 2 and 3. The cross sections measured in π^- scattering are larger than those measured in π^+ scattering at both energies. Proton and neutron matrix elements extracted for the 3_1^- state (using the Tassie model) at the two energies are the same within our uncertainties. Surprisingly, the proton matrix elements obtained through the vibrational model for this 3_1^- transition show a significant energy dependence, as seen from the values in Table I. Their average from the two ener-

TABLE I. Multipole matrix elements (proton and neutron/proton ratios) extracted for ^{208}Pb from this work using both the Tassie and vibrational (derivative) forms of the collective model. In the simplest collective model the ratio $M_n/M_p=N/Z=1.54$.

State (J^π)	Extr (MeV)	T_π (MeV)	M_p (Tassie) (fm^l)	M_n/M_p (Tassie)	M_p (vibrat) (fm^l)	M_n/M_p (vibrat)
3_1^-	2.61	120	752(41)	1.85(0.14)	648(35)	2.45(0.18)
		250	772(65)	1.68(0.18)	830(70)	1.81(0.18)
3_2^-	4.70	120	280(48)	1.28(0.32)	252(48)	1.69(0.35)
		250	233(27)	1.44(0.30)	258(30)	1.46(0.30)
3_3^-	5.30	120	321(80)	1.24(0.34)	283(71)	1.68(0.46)
		250	285(28)	1.45(0.21)	296(29)	1.60(0.25)
4^+	4.32	120	43(4)E+02	1.44(0.18)	37(3)E+02	1.86(0.22)
		250	42(5)E+02	1.33(0.23)	46(5)E+02	1.39(0.20)
5_1^-	3.20	120	19(1)E+03	2.84(0.26)	19(1)E+03	2.68(0.21)
		250	22(2)E+03	1.91(0.25)	20(2)E+03	1.99(0.32)
5_2^-	3.71	120	12(2)E+03	2.50(0.53)	8(2)E+03	4.1(1.9)
		250	16(3)E+03	1.63(0.40)	16(3)E+03	1.69(0.45)
6^+	4.42	120	24(3)E+04	1.83(0.74)	16(4)E+04	2.25(0.64)
		250	32(5)E+04	1.09(0.28)	28(6)E+04	1.00(0.24)

gies, using this model, are near those found using the Tassie model. The neutron matrix elements from both analyses agree at the two energies, and show little difference between the two models. There is but little difference between the shapes predicted with the two collective models, as noted in Figs. 4 and 5.

Calculations using the Tassie model, plotted with the data for the 3_1^- state in Figs. 2 and 3, provide a good description of the data at $T_\pi = 120$ MeV. At $T_\pi = 250$ MeV the position of the minimum is reproduced but the magnitude of the second maximum is not correctly predicted. The larger neutron diffusivity produces slightly better agreement with the data at both energies. The values of M_p, M_n, and M_n/M_p calculated from the resulting fits are listed in Table I.

Our data at two pion energies populating the 3_2^- (4.70 MeV) and 3_3^- (5.30 MeV) states are compared to DWIA calculations using the two collective models in Figs. 4 and 5. There is no preference for the shape obtained from either model. Extracted matrix elements are listed in Table I. All three 3^- states exhibit Tassie-model M_n/M_p ratios near the collective expectation of $N/Z = 1.54$, but as Table I shows, the phonon vibrational-model results show the 3_1^- transition to have an average ratio of M_n/M_p notably larger than N/Z.

The angular distributions extracted for the transitions to the 5_1^- (3.20 MeV) and 5_2^- (3.70 MeV) states are plotted in Fig. 4 (at $T_\pi = 120$ MeV) and Fig. 5 (at $T_\pi = 250$ MeV). As was the case for the 3_1^- state, the peak cross sections for π^- scattering are larger than those for π^+ scattering. The calculations using Tassie-model or

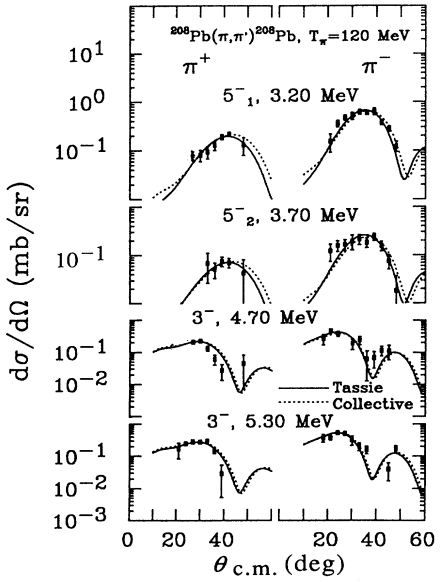

FIG. 4. ^{208}Pb $(\pi,\pi')^{208}$Pb 5^- and 3^- inelastic-scattering angular distributions at $T_\pi = 120$ MeV. The solid curves represent Tassie-model $l = 3$ and 5 DWPI calculations and the dotted curves represent vibrational (derivative form factor) calculations.

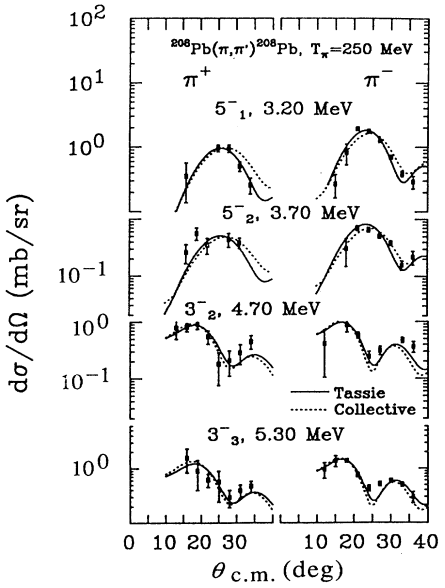

FIG. 5. ^{208}Pb $(\pi,\pi')^{208}$Pb 5^- and 3^- inelastic-scattering angular distributions at $T_\pi = 250$ MeV. The solid curves represent Tassie-model $l = 3$ and 5 DWPI calculations and the dotted curves represent vibrational (derivative form factor) calculations.

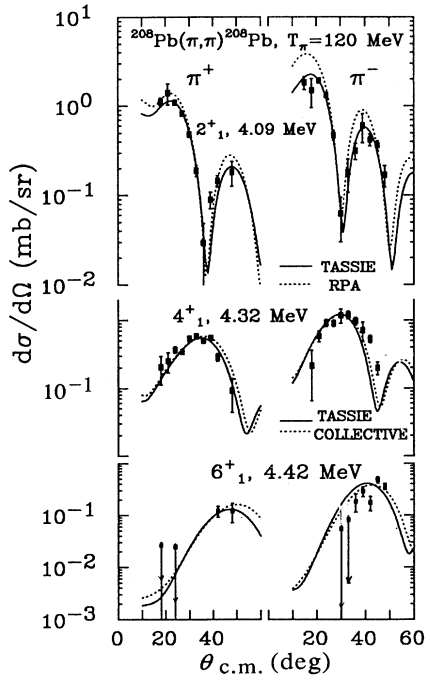

FIG. 6. ^{208}Pb $(\pi,\pi')^{208}$Pb 2_1^+, 4_1^+, and 6_1^+ inelastic-scattering angular distributions at $T_\pi = 120$ MeV. The solid curves represent Tassie-model $l = 2$, 4, and 6 DWPI calculations, and the dotted curves represent RPA predictions for the 2^+ state and vibrational (derivative form factor) calculations for the other states.

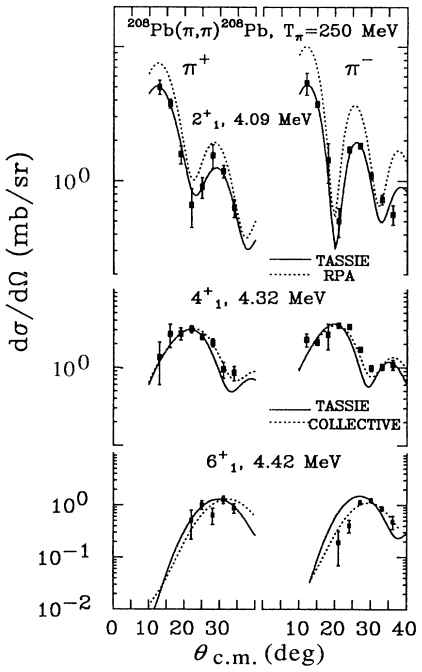

FIG. 7. ^{208}Pb $(\pi,\pi')^{208}$Pb 2^+_1, 4^+_1, and 6^+_1 inelastic-scattering angular distributions at T_π=250 MeV. The solid curves represent Tassie-model l=2, 4, and 6 DWPI calculations, and the dotted curves represent RPA predictions for the 2^+ state and vibrational (derivative form factor) calculations for the other states.

vibrational-model transition densities describe the shapes of these data equally well, possibly due to the large uncertainties in the data and the limited angular range of the data. Matrix elements are listed in Table I.

Collective model transition densities give the DWIA curves compared in Figs. 6 and 7 to data for the 2^+_1 (4.09 MeV), 4^+_1 (4.32 MeV), and 6^+_1 (4.42 MeV) states. The vibrational calculation is very similar to the Tassie calculation for the 2^+ transitions, and is not shown. At 120 MeV there is little to prefer either model by shapes alone, but the Tassie results must be preferred at 250 MeV for the 4^+ and 6^+ data. Matrix elements for the 4^+ state agree for the two beam energies when extracted with the Tassie model for the scattering, with less agreement using the phonon model. This is also the case for the 6^+ analysis, but with large uncertainties. The high power of the radius for the Tassie model for a 6^+ transition makes the two models greatly different for this instance.

Angular distributions for the 2^+_1 state are plotted in Fig. 6 (at 120 MeV) and Fig. 7 (at 250 MeV). Plotted along with the data in Figs. 6 and 7 are calculations using a Tassie model transition density with the deformation parameters adjusted to give the best fit to the π^+ and π^- data (solid curve). These calculations fit the data very well over the entire angular range. Matrix elements from the two collective analyses are listed in Table II, where good agreement is found with either model between the two beam energies.

TABLE II. Model dependence of the 2^+_1 (4.09 MeV) matrix elements for ^{208}Pb from this work. The M_p value found from electron scattering is 56±3 fm^2 from Ref. [10], while 48 fm^2 is reported from alpha scattering in Ref. [29].

Model	T_π (MeV)	M_p (fm^2)	M_n (fm^2)	M_n/M_p
RPA[a]	120	55	83	1.51
	250	55	83	1.51
RPA[b]	120	57(3)	68(5)	1.19(0.11)
	250	48(3)	61(5)	1.27(0.13)
Vibration	120	55(3)	96(7)	1.75(0.16)
	250	56(3)	96(8)	1.71(0.17)
Tassie	120	55(3)	90(7)	1.64(0.16)
	250	54(3)	86(6)	1.59(0.14)

[a]RPA prediction from Ref. [27].
[b]Values needed to fit data using RPA transition shape.

For this 4.09 MeV 2^+ state we also used RPA transition densities from Ref. [27] to calculate DWIA cross sections since these differ significantly for protons and neutrons, in contrast to the collective models. These densities are compared in Fig. 8, while the DWIA calculations are compared to the 2^+_1 data at the two beam energies in Figs. 6 and 7. Although the diffractive shapes agree with the data, the magnitudes do not agree with those observed, especially for π^-. Matrix elements from these RPA calculations are listed in Table II, where agreement is found with the collective results for M_p. This is a reflection of the near agreement between calculation and data for π^+ scattering.

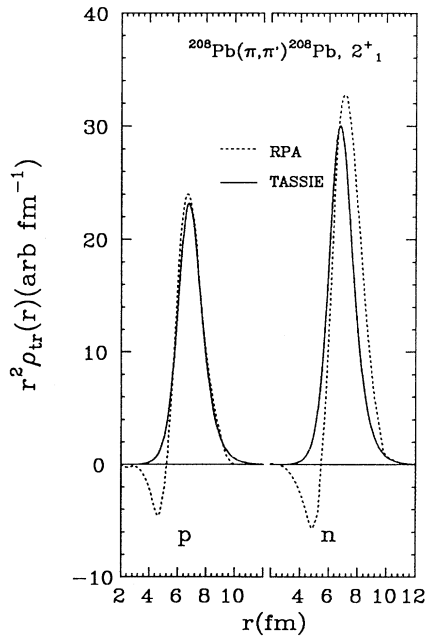

FIG. 8. Comparisons of Tassie and RPA transition density shapes (neutron and proton) for the first 2^+ state [27]. The Tassie densities are scaled by the deformation β in order to compare the shapes, and hence those units are arbitrary.

We have also used the RPA transition densities with magnitudes scaled to fit the data, using different scale factors for neutron and proton components. The resulting fits are very comparable to those using the Tassie model, but yield the matrix elements listed in Table II. Little change is found from the original RPA value for M_p, but M_n is greatly decreased. We must conclude that the neutron portion of the RPA model in Ref. [27] is inadequate, but difficult to observe by any means except inelastic pion scattering. Similar comparisons of π^- and π^+ scattering for other 2_1^+ states have found neutron matrix elements larger than those of the collective model, but in this example the RPA overpredicts the π^- cross section.

VI. COMPARISON TO OTHER PROBES AND ENERGY DEPENDENCE

Matrix elements for transitions in ^{208}Pb have also been determined from the scattering of other probes. Comparisons using baryon scattering have found M_n/M_p ratios ranging from 1.3 to 1.6 for the 2.61 MeV 3_1^- transition, while 1.5 is found for the 2_1^+ 4.09 MeV state [17,18,28,30]. These ratios are close to the Tassie-model results extracted from this work (Table III), which are also near $N/Z=1.54$, as expected for a hydrodynamic model. It is an interesting result that such an agreement among different probes is found for these low-lying states, while for the strong sum-rule exhausting giant-resonance quadrupole transition in ^{208}Pb the pion scattering shows less proton strength than predicted or suggested by a compilation of proton- and neutron-scattering data [7].

In the hydrodynamic model, isoscalar inelastic alpha-particle scattering can be used to obtain M_p by assuming $M_p=ZM_0/A$, where the isoscalar matrix element M_0 is obtained from the deformation lengths βR_0. Using derivative form factors to match those used in the alpha-scattering analysis, the deformation lengths listed in Ref. [29], and the matter parameters used in this work, we compute and list the resulting proton matrix elements in Table III. Again, in most cases, these results are similar to both the electromagnetic and the pion-scattering analysis.

Agreement overall between the energy-averaged Tassie pion results and the electro-magnetic results is very good, with the ratio of pion-to-electromagnetic strengths for seven strong states averaging 0.97 ± 0.07. Agreement is not as good for energy-averaged derivative pion results, with an average of 0.90 ± 0.10, and the worst for alpha scattering, with a ratio to the electromagnetic matrix elements of 0.79 ± 0.22. Variances for seven transitions are quoted as the uncertainties.

If the correct excitation model (transition density) and reaction model are used to extract the matrix elements, then these should remain independent of the initial beam energy, as well as that of the projectile. This dependence of the M_n/M_p ratios on T_π for the low-lying states in ^{208}Pb is shown in Fig. 9 as well as through the tables. Data at other pion beam energies [14,15] are included as well, with a new analysis using the methods described above for consistency.

Here we see that the strongest state, the first 3^-, has matrix elements that are independent of energy, to within our uncertainties, if the Tassie-model description is used. In the vibrational model, however, there is a consistently lower relative neutron contribution at higher pion ener-

TABLE III. Comparison of proton multipole matrix elements extracted by collective models for ^{208}Pb from electromagnetic measurements, from this work, and from alpha-particle scattering, as described in the text. The pion results from this work are given as an energy average and all units are in fm^l.

State (J^π)	E_x (MeV)	$M_p(EM)$[a]	$M_p(\alpha,\alpha')$[b] (vibration)	$M_p(\pi,\pi')$[c] (Tassie)	$M_p(\pi,\pi')$[c] (vibration)
3^-	2.61	784[d]	808	762	739
	4.70		164	256	267
	5.30	360	199	303	289
4^+	4.32	$39.4E+02$	$33.1E+02$	$42.5E+02$	$41.1E+02$
5^-	3.20	$21.1E+03$	$20.6E+03$	$20.5E+03$	$19.5E+03$
	3.71	$15.5E+03$	$13.1E+03$	$14.0E+03$	$12.0E+03$
6^+	4.42	$25.8E+04$	$11.1E+04$	$28.0E+04$	$22.0E+04$

[a]Values from electron scattering [10,20].
[b]Values from alpha scattering [29].
[c]Values from this work.
[d]Reference [30].

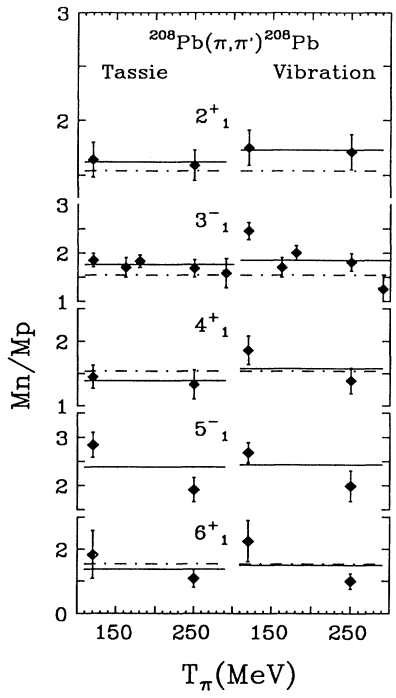

FIG. 9. Energy dependence of the M_n/M_p ratios obtained with both Tassie and vibrational collective models. The states are labeled according to Table I where the dashed lines are the $N/Z=1.54$ collective predictions and the solid lines are in an energy average to guide the eye. The 3_1^- results are from this work and from the results of Ref. [16] where the 162, 180, and 291 MeV data of Refs. [14,15,12] were analyzed using the methods of this paper.

gies. Because the pions sample different sections of the nucleus at different energies, this possible energy dependence may indicate an inadequacy with the shape of the vibrational transition density for these states. This is a surprise because it is expected that the first 3^- state would be largely vibrational. A similar situation occurs for the first 4^+ state, though the errors are larger and hence the results are not as convincing.

Both the vibrational and Tassie-model calculations, however, clearly give results that are independent of energy for the first 2^+ state. This is also true when analyzed in the renormalized RPA. A trend can be seen in first 5^- and 6^+ states, however, where there is a lower relative neutron contribution at higher energies. This situation is not improved when the neutron diffuseness is raised to the value that optimally fits the elastic distribution. This trend is also not due to an uncompensated Coulomb-nuclear interference effect because the 2_1^+ state, which is expected to have the strongest Coulomb excitation amplitude, shows no variation with T_π. Coulomb excitation was included in the DWIA analyses that provide the matrix elements shown in all cases

VII. CONCLUSION

When data from pion ^{208}Pb scattering are analyzed using vibrational and Tassie forms of the collective model the angular distributions are adequately reproduced. The RPA model also adequately reproduces the shapes for the 2_1^+ data but overpredicts the neutron (π^-) cross sections for this transition.

The resulting neutron and proton matrix elements for the strong low-lying states are in good agreement with those extracted using other probes and are in agreement with the N/Z hydrodynamic prediction, where the Tassie model is in slightly better agreement. This result is particularly interesting in light of recent pion-scattering measurements of the giant resonances in ^{208}Pb which are not in agreement with the neutron strength parameters extracted from neutron and proton scattering.

From the matrix element extraction here, however, the relative neutron contributions to the low-lying states typically drop systematically with initial pion energy when extracted from a vibrational model, but generally do not when a Tassie analysis is employed, suggesting that the Tassie shape is unexpectedly more reliable than the simple derivative in these cases. This type of energy independence has been observed for lighter nuclei using the simple vibrational model, and it now appears that this matrix element extraction is also independent of energy for most of the low-lying states of ^{208}Pb.

ACKNOWLEDGMENTS

This work was supported in part by the U.S. Department of Energy and the Robert A. Welch Foundation. We thank D. Crockett, A. H. Fuentes, M. Lynker, and M. A. Machuca from the University of Texas for their help in data taking.

*Present address: Lewis and Clark College, Portland, OR 97219.

†Present address: MIT Bates, Middleton, MA 01949-2846.

[1] C. L. Morris *et al.*, Phys Rev. C **35**, 1388 (1987).
[2] D. S. Oakley *et al.*, Phys. Rev. C **35**, 1392 (1987).
[3] S. Mordechai *et al.*, Phys. Rev. C **36**, 710 (1987).
[4] K. G. Boyer *et al.*, Phys. Rev. C **24**, 598 (1981).
[5] D. S. Oakley and H. T. Fortune, Phys. Rev. C **37**, 1126 (1988).
[6] W. B. Cottingame *et al.*, Phys. Rev. C **36**, 230 (1987).
[7] S. J. Seestrom-Morris, C. L. Morris, J. M. Moss, T. A. Carey, D. Drake, J. Dousse, L. C. Bland, and G. S. Adams, Phys. Rev. C **33**, 1847 (1986).
[8] E. L. Hjort *et al.*, Phys. Rev. Lett. **62**, 870 (1989).
[9] M. B. Lewis, F. E. Bertrand, and D. J. Horen, Phys. Rev. C **8**, 398 (1973); F. E. Bertrand and D. C. Kocher, *ibid.* **13**, 2241 (1976).
[10] J. Heisenberg, J. Lichtenstadt, C. N. Papanicolas, and J. S. McCarthy, Phys. Rev. C **25**, 2292 (1982).
[11] G. A. Rinker and J. Speth, Nucl. Phys. **A306**, 360 (1978).
[12] D. F. Geesaman *et al.*, Phys. Rev. C **23**, 2635 (1981).
[13] J. Arvieux, J. P. Albanese, J. Bolger, E. Boschitz, C. H. Q. Ingram, L. Pflug, J. Jansen, J. Zichy, E. Rost, and A. S. Rosenthal, Nucl. Phys. **A312**, 368 (1978).
[14] C. Olmer *et al.*, Phys. Rev. C **21**, 254 (1980).
[15] S. J. Seestrom-Morris *et al.* (unpublished).
[16] D. S. Oakley, P. D. Kunz, and C. L. Morris, Phys. Rev. C **41**, 1081 (1990).
[17] S. Kailas, Phys. Rev. C **35**, 2324 (1987).
[18] M. Gazzaly, N. M. Hintz, G. S. Kyle, R. K. Owen, G. W. Hoffman, M. Barlett, and G. Blandpied, Phys. Rev. C **25**, 408 (1982).
[19] G. Rowe, M. Salomon, and R. H. Landau, Phys. Rev. C **18**, 584 (1978).
[20] M. J. Martin, Nucl. Data Sheets **47**, 797 (1986).
[21] R. A. Eisenstein and G. A. Miller, Comput. Phys. Commun. **11**, 95 (1976).
[22] L. S. Kisslinger, Phys. Rev. **98**, 761 (1955).
[23] W. B. Cottingame and D. B. Holtkamp, Phys. Rev. Lett. **45**, 1828 (1980).
[24] L. J. Tassie and F. C. Barker, Phys. Rev. **111**, 940 (1958).
[25] H. Ui and T. Tsukamoto, Prog. Theor. Phys. **51**, 1377 (1974).
[26] G. R. Satchler, *Introduction to Nuclear Reactions* (Wiley, New York, 1980), p. 210.
[27] J. Wambach, F. Osterfeld, J. Speth, and V. A. Madsen, Nucl. Phys. **A324**, 77 (1979).
[28] V. A. Madsen, T. Suzuki, A. M. Bernstein, and V. R. Brown, Phys. Lett. **123B**, 13 (1983).
[29] M. N. Harakeh, B. Van Heyst, K. Van der Borg, and A. Van der Woude, Nucl. Phys. **A327**, 373 (1979).
[30] D. Goutte *et al.*, Phys. Rev. Lett. **45**, 1618 (1980).